Integrated, high-throughput, multiomics platform enables data-driven construction of cellular responses and reveals global drug mechanisms of action

Norris, Jeremy L.; Farrow, Melissa A.; Gutierrez, Danielle B.; Palmer, Lauren D.; Muszynski, Nicole; Sherrod, Stacy D.; Pino, James C.; Allen, Jamie L.; Spraggins, Jeffrey M.; Lubbock, Alex L.R.

DOI
10.1021/acs.jproteome.6b01004

Publication date
2017

Document Version
Final published version

Published in
Journal of Proteome Research

Journal of proteome research

Article

pubs.acs.org/jpr

Integrated, High-Throughput, Multiomics Platform Enables Data-Driven Construction of Cellular Responses and Reveals Global Drug Mechanisms of Action

Jeremy L. Norris,[†,‡,∇,○] Melissa A. Farrow,[⊗] Danielle B. Gutierrez,[†,‡] Lauren D. Palmer,[⊗] Nicole Muszynski,[¶,■] Stacy D. Sherrod,[∇,¶,◒,◆] James C. Pino,[§,◇] Jamie L. Allen,[†,‡] Jeffrey M. Spraggins,[†,‡,∇] Alex L. R. Lubbock,[§] Ashley Jordan,[⊗] William Burns,[⊗] James C. Poland,[∇,◒,◆] Carrie Romer,[†,‡] M. Lisa Manier,[†,‡] Yuan-wei Nei,[†,‡] Boone M. Prentice,[†,‡] Kristie L. Rose,[†,‡] Salisha Hill,[†,‡] Raf Van de Plas,[†,‡,∫] Tina Tsui,[†,‡] Nathaniel M. Braman,[●] M. Ray Keller,[∇,◒,◆] Stacey A. Rutherford,[⊗] Nichole Lobdell,[⊗] Carlos F. Lopez,[○,§,●,‖] D. Borden Lacy,[‡,⊗] John A. McLean,[∇,¶,◒,◆] John P. Wikswo,[○,¶,●,⊥,⌀] Eric P. Skaar,[⊗] and Richard M. Caprioli*[,†,‡,∇,○,#,□]

[†]Mass Spectrometry Research Center, [‡]Biochemistry, [§]Cancer Biology, [‖]Biomedical Informatics, [⊥]Molecular Physiology and Biophysics, [#]Pharmacology, and [□]Medicine, Vanderbilt University School of Medicine, Nashville, Tennessee 37240, United States

[∇]Chemistry, [○]Vanderbilt-Ingram Cancer Center, [¶]Vanderbilt Institute for Integrative Biosystems Research and Education, and [◒]Center for Innovative Technology, [⌀]Physics, Vanderbilt University, Nashville, Tennessee 37235, United States

[⊗]Pathology, Microbiology & Immunology, [■]Surgery, and [◇]Chemical and Physical Biology Graduate Program, Vanderbilt University School of Medicine, Nashville, Tennessee 37232, United States

[◆]Vanderbilt Institute of Chemical Biology, Vanderbilt University, Nashville, Tennessee 37232, United States

[∫]Delft Center for Systems and Control, Delft University of Technology, Delft 2628 CD, The Netherlands

[●]Biomedical Engineering, Vanderbilt University School of Engineering, Nashville, Tennessee 37235, United States

Supporting Information

ABSTRACT: An understanding of how cells respond to perturbation is essential for biological applications; however, most approaches for profiling cellular response are limited in scope to pre-established targets. Global analysis of molecular mechanism will advance our understanding of the complex networks constituting cellular perturbation and lead to advancements in areas, such as infectious disease pathogenesis, developmental biology, pathophysiology, pharmacology, and toxicology. We have developed a high-throughput multiomics platform for comprehensive, de novo characterization of cellular mechanisms of action. Platform validation using cisplatin as a test compound demonstrates quantification of over 10 000 unique, significant molecular changes in less than 30 days. These data provide excellent coverage of known cisplatin-induced molecular changes and previously unrecognized insights into cisplatin resistance. This proof-of-principle study demonstrates the value of this platform as a resource to understand complex cellular responses in a high-throughput manner.

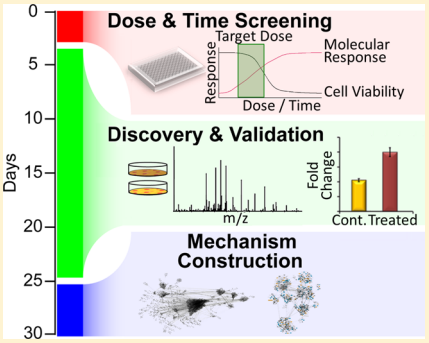

KEYWORDS: *cisplatin, drug discovery, high-throughput, mechanism of action, omics*

INTRODUCTION

Comprehensive analysis of cellular responses at the molecular level facilitates a rich understanding of the complexity and dynamic nature of cellular pathways. While initial studies of cellular exposure to exogenous compounds often explain a primary mechanism of action (MOA), many of these complexities and secondary MOAs are not understood or even anticipated until several years after early discoveries. This is exemplified by the identification of thalidomide's target of toxicity 50 years after observance of the teratogenic properties.[1] Even therapeutic compounds designed for specific targets, for example statins, often induce multifaceted effects.[2] Thus, there is a need to expand upon the way we evaluate cellular response to perturbations.

Conversely, drug development strategies largely focus on the interaction of a drug candidate with a single molecular target, assuming that optimization of affinity to a target produces the most effective outcomes. Preclinical research has been optimized,

Received: November 23, 2016
Published: January 14, 2017

DOI: 10.1021/acs.jproteome.6b01004
J. Proteome Res. 2017, 16, 1364−1375

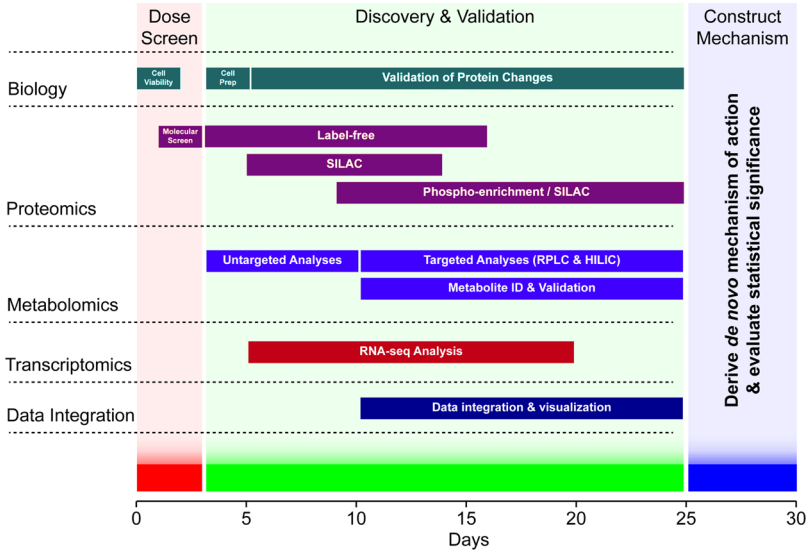

Figure 1. Multiomics platform for MOA construction. The 30 day procedure has three distinct phases: dose screen (days 0−3), discovery and validation (days 4−25), and mechanism construction (days 26−30). Phase 1 incorporates cell viability and molecular screens to establish protocols for the discovery phase. Phase 2 integrates proteomics, metabolomics, and transcriptomics to determine molecular changes correlated with compound dose. In Phase 3, network analysis of all statistically significant changes drives construction of a comprehensive MOA.

automated, and structured to generate drug candidates at increasingly rapid rates; yet, the failure rate remains high. Recent estimates suggest that as few as one in ten developed drug candidates succeed.[3−5] Factors leading to failure include safety concerns and effects that are difficult to predict with targeted assays.[3,5] These undesirable side effects may not manifest until late stages of clinical trials, after investing billions of dollars into a lead compound.[6,7]

A decline in research and development efficiency for the development of new drugs is well-documented.[8−10] One contributing factor to those failures is that current technologies do not provide a systems-level evaluation of the candidate drug.[11] In contrast, it has been noted that drug development was more effective in the era when animals (e.g., systems) were primarily used in the initial stages of development,[8] emphasizing the tradeoffs in using a reductionist approach to drug development. Clearly, there is an urgent need to fundamentally change the way we analyze cellular responses and evaluate potential therapeutic drugs and threatening toxins. A comprehensive approach to understanding cellular response to drug candidates can contribute to both the efficacy and safety of the final product, elucidate pathways of adaptive tolerance and resistance, and highlight possible polypharmacological applications. Additionally, a complete understanding of the molecular landscape allows for the screening of pre-existing mutations that dispose patients to therapeutic failure.

To understand a multifaceted cellular response up front requires exhaustive molecular profiling, a task well-suited to omics approaches. The prevailing dogma for these technologies is that they are not applicable to programs requiring high-throughput results.[12,13] However, recent advances in the technologies used for transcriptomics, proteomics, and metabolomics provide unprecedented molecular specificity and speed while maintaining high standards for data quality. Integration of these technologies facilitates a cohesive analysis of cellular response, and increases in analytical efficiency coupled with modern computational capabilities make it feasible to rapidly obtain comprehensive data of a compound's MOA. Of equal importance, this approach enables the discovery of cellular processes outside of targeted pathways, providing molecular information and insight into complex cellular responses.

Here, we describe an integrated analytical and computational approach that empirically derives a global MOA for a compound in less than 30 days. We demonstrate proof-of-principle for this technology platform using cisplatin, a well-established DNA damage-inducing chemotherapeutic. Research over the past 20 years establishes a few dozen compounds implicated in cisplatin's primary MOA. In 30 days, this platform quantified over 10 000 unique molecular changes, including 55% of the species in an expanded canonical network. Importantly, the data captured novel pathways that may inform clinical observations of cisplatin resistance. A driving aim for this technology is to move beyond the limits of targeted analyses informed by established pathways and to provide a technology for the accelerated understanding of MOA.

EXPERIMENTAL PROCEDURES

Cell Culture

A549 cells were cultured in DMEM or stable isotope labeling with amino acids in cell culture (SILAC) DMEM (Thermo Scientific) and treated with 50 μM cisplatin (Tocris Bioscience) or ddH_2O.

Screening

Cell viability and apoptosis were assessed by CellTiter Glo (Promega) and ApoONE (Promega) kits, respectively. Molecular changes were screened using a matrix-assisted laser desorption−ionization Fourier-transform ion cyclotron resonance (MALDI-FTICR) MS platform.

Multiomics Analysis

Samples were analyzed for transcriptome changes by RNA sequencing at the Genomics Services Lab, HudsonAlpha, for proteome changes by label-free, SILAC, and phospho-enriched SILAC liquid chromatography−tandem mass spectrometry (LC−MS/MS), and metabolome changes by ultraperformance liquid chromatography−ion mobility mass spectrometry (UPLC−IM-MS) and data-independent acquisition (MSE) using both hydrophilic-interaction liquid chromatography and reverse-phase liquid chromatography.

DOI: 10.1021/acs.jproteome.6b01004
J. Proteome Res. 2017, 16, 1364−1375

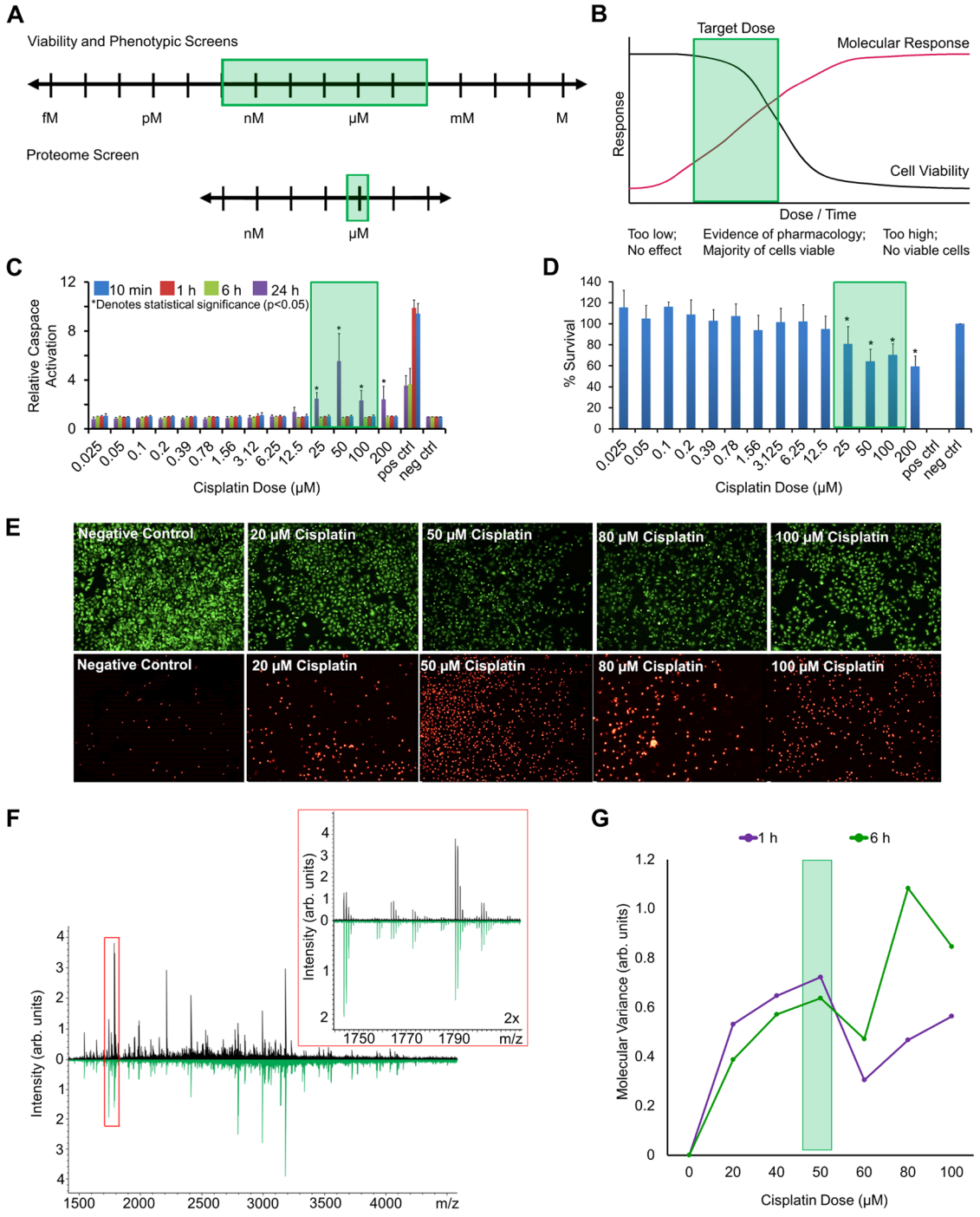

Figure 2. Phase 1: dose screening (days 0−3). (A) Two different stages of the screening are illustrated. The phenotypic screens evaluate physiological changes to narrow the dose to a small number of responsive conditions. The molecular screen focuses these possibilities to the optimal conditions. The green boxes represent theoretical dose ranges. (B) This cartoon conceptualizes our approach to determine optimal dosing conditions. The green box highlights the ideal target dose range, one that stimulates the greatest molecular response while maintaining a tolerable level of cell viability. (C,D) Phenotypic screening results for cisplatin at 24 h show (C) relative caspase activation (ApoONE) and (D) cell viability (CellTiter Glo). The green boxes demonstrate effective responses. (E) Qualitative evaluation of the cell viability at 24 h confirms an optimal dose range. Green, live cells; red, dead cells. Note that brightness was enhanced by 60% for all lower panels to improve visibility of the red pixels. (F) MALDI FTICR MS spectra from a 6 h exposure illustrate molecular differences in control (top, black) and 50 μM cisplatin-treated samples (bottom, green). The inset highlights differences in the molecular signatures of the control and treated samples within a selected m/z region (see asterisks). (G) This graph summarizes the results of the molecular screen. The green box indicates the selected dose for Phase 2 discovery experiments.

Computational Analysis and Data Mining

Data from all platforms were integrated and parsed for significantly changed, unique species. We developed an analysis pipeline (manuscript in preparation) implemented in the Python programming language as part of the PySB modeling framework.[14] Bioservices[15] was used to download pathways from the KEGG database[16] that contain any proteins from a list of seed species. These pathways were combined to form a unified

DOI: 10.1021/acs.jproteome.6b01004
J. Proteome Res. 2017, 16, 1364−1375

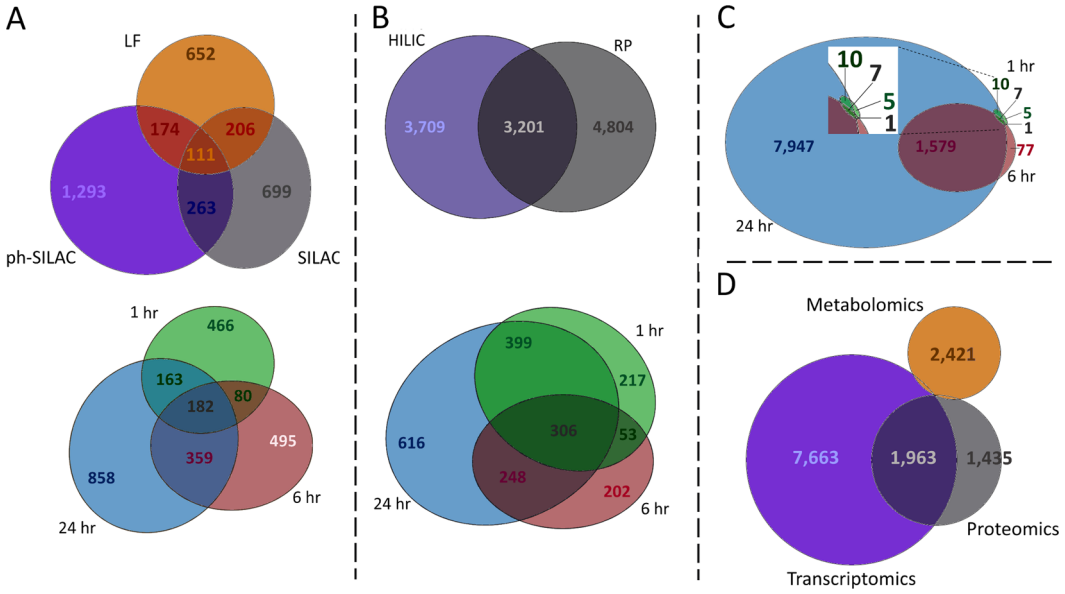

Figure 3. Phase 2: discovery results (days 4−25). (A) Significantly changed proteins (determined based on gene symbol) and (B) identified (top) and significantly changed (bottom) metabolites show the overlap across the modalities and time. For visual simplicity, 3 out of 4 time points are shown. Abbreviations: LF, label-free; HILIC, hydrophilic liquid interaction chromatography; RP, reverse-phase chromatography. (C) Transcriptomic data show the overlap of significantly changed transcripts across time. (D) A cross-platform comparison of unique, significantly changed species shows the overlap between transcriptomics and proteomics.

network based on common protein species. To examine the species-to-species interactions in our data networks, we used the open source systems biology platform Cytoscape,[17] the QIAGEN IPA network analysis tool, and annotated literature.

RESULTS AND DISCUSSION

This study validates a multiomics platform designed to assess the comprehensive MOA of exogenous compounds in 30 days. We considered selection of cell type, exposure methods, and analytical modalities by evaluating stability, reproducibility, utility, and feasibility within 30 days. For this study, we used A549 cells; however, our platform is amenable to various adherent and suspension cell lines. The sponsoring agency selected cisplatin as the test compound and revealed its identity on the first day of the 30 day period.

Figure 1 graphically illustrates the three phases of our procedure: (1) molecular screening (days 0−3), (2) discovery analytics (days 4−25), and (3) mechanism construction (days 26−30). Phase 1 screens a wide range of cisplatin dose and exposure times to establish the treatment protocol for discovery experiments. This preliminary screen deduces dosing conditions that provide relevant data for the MOA, allowing the application of this protocol to uncharacterized compounds. During Phase 2, transcriptomics, proteomics, and metabolomics determine changes in molecular expression correlated with exposure to the compound. In Phase 3, data integration and analysis drive mechanism construction.

Phase 1: Preliminary Screening Determination of Relevant Dose and Exposure Time

To make the analysis strategy applicable to uncharacterized compounds, it does not rely on previous experimental data to establish an exposure dose. We hypothesized that a preliminary screening process (Figure 2) could select optimal treatment conditions for Phase 2 omics experiments. Figure 2A illustrates the two-stage screening protocol. First, a set of assays that indicate physiological perturbations (e.g., cell viability, cell cycle arrest, oxidative stress, etc.) narrows the possible dose range to a small number of conditions. Second, mass spectrometry (MS) analysis of proteome changes within this limited dose range leads to the selection of a single dose condition for all subsequent experiments. The optimal dose, conceptualized in Figure 2B, elicits maximum molecular response while preserving >50% cell viability.

During Stage 1 of the screening experiment, we monitored dose-dependent caspase 3/7 activation (Figure 2C), ATP levels (Figure 2D), and cell viability (Figure 2E). We analyzed 14 doses (0.025−200 μM) for cisplatin exposure times of 10 m and 1, 6, and 24 h, with some selected measurements at 48 and 96 h. On the basis of the results obtained on day 1, the dose range of 20−100 μM was prepared for molecular screening.

For Stage 2, we developed a rapid proteome screen using matrix-assisted laser desorption ionization (MALDI) MS to evaluate the magnitude of the molecular response. This assay determines changes in MS profiles at selected conditions compared to the control, ensuring maximum opportunity to observe significant molecular changes in the discovery phase. To maximize throughput, we focused on profile changes rather than identifications, avoiding the use of chromatography and tandem MS. These results titrated the cisplatin dose used in later experiments but were not used in the construction of the cisplatin MOA.

Figure 2F shows representative mass spectra from this experiment, a 6 h exposure of 50 μM cisplatin and a vehicle control. Each peptidic profile contained >4000 unique mass-to-charge (m/z) peaks to monitor for intensity changes across exposure conditions. To determine which cisplatin dose induced the greatest molecular change, we developed a quantitative, automated approach to determine a molecular variance score—a metric that projects the high-dimensional variance between the spectra of different experimental conditions to a lower-dimensional

DOI: 10.1021/acs.jproteome.6b01004
J. Proteome Res. 2017, 16, 1364−1375

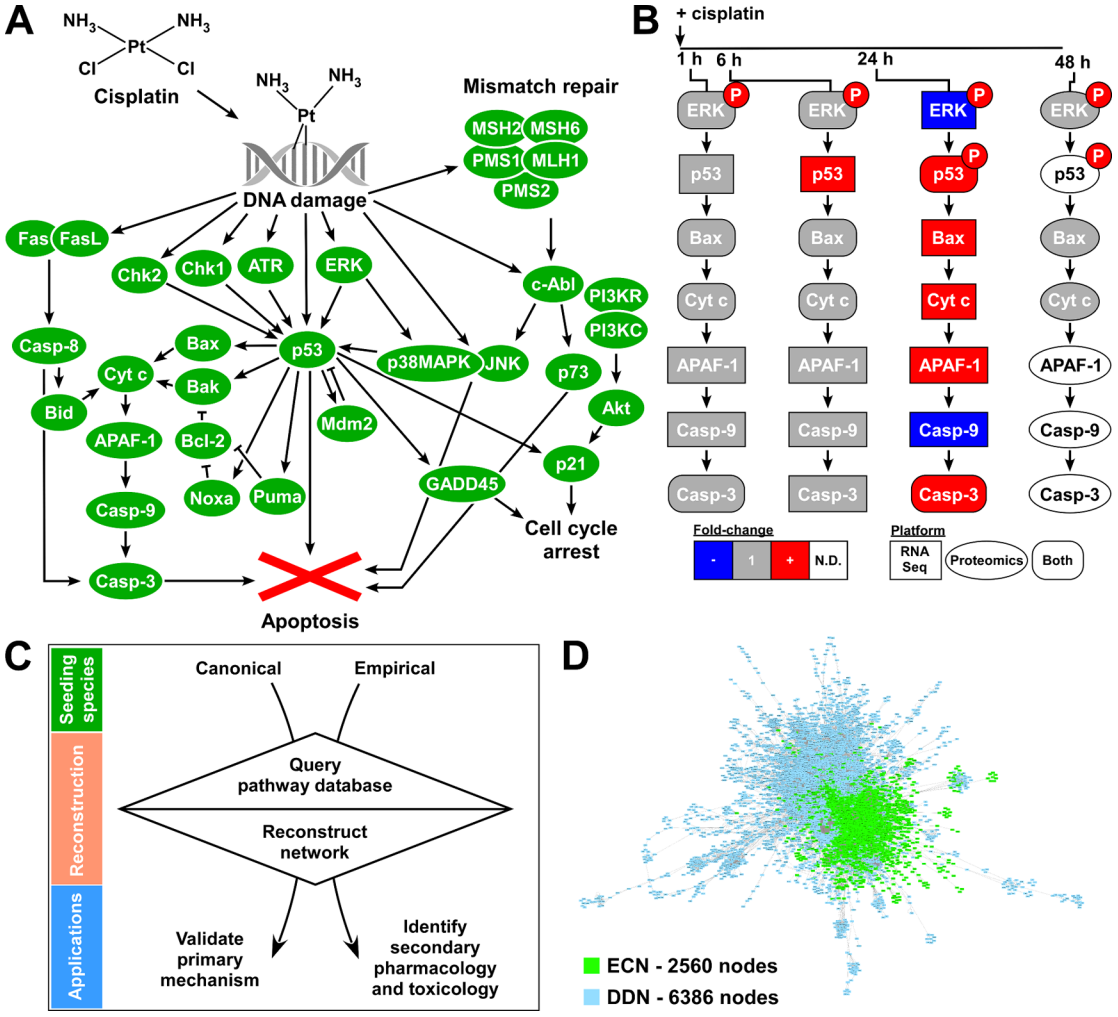

Figure 4. Phase 3: mechanism construction (days 26−30). (A) The cisplatin canonical MOA generated from a literature survey (green). (B) A vignette of the intrinsic apoptosis pathway illustrates directional fold changes and detection status from the empirical data. Abbreviations: ERK, ERK1/2; ERKP, ERK1 pThr202/pTyr204 and ERK2 pThr185/pTyr187; and p53P, p53 pSer392. (C) This workflow conceptualizes the reconstruction of networks from seeding species. (D) An overlay of the ECN (green) and the DDN (blue) demonstrates the comprehensive nature of empirical mechanism construction beyond the canonical mechanism.

representation using a principle component analysis. These details are in the supplemental methods.

Figure 2G shows the molecular variance score for each cisplatin dose measured at 1 and 6 h. Only exposure times <24 h were analyzed during the molecular screen to maintain an efficient screening period (≤3 days). We observed an increase in molecular variance with increasing cisplatin dose up to 50 μM; greater doses did not show a correlated response. This instability in the molecular variance score at doses >50 μM at 1 and 6 h corresponds with the variation seen in the caspase activation assay in the same dose range at 24 h (Figure 2C). In both the physiological and molecular screen, 50 μM cisplatin elicits a maximum response and maintains cell viability of >50%, indicating an optimal dose of 50 μM cisplatin for discovery experiments.

This screen-determined concentration compares with reports of cisplatin-induced apoptosis and cytotoxicity; exposure doses range from 3.3 to 1000 μM (Figure S1), and the IC_{50} for A549 cells is 18−64 μM.[18,19] The molecular screen confirmed cisplatin-induced toxicity is measurable at 50 μM and as early as 1 h. These results support our hypothesis that a preliminary screen can determine optimal treatment conditions for an unknown compound, and they validate our established workflow.

Phase 2: A Multi-Omics Platform Capture of Cisplatin-Induced Molecular Perturbations

During the discovery phase, we acquired comprehensive molecular data from transcriptome, proteome, phosphoproteome, and metabolome measurements of A549 cells treated with 50 μM cisplatin for 1, 6, 24, and 48 h. In total, we collected 254 470 measurements (which represents approximately 10 s per measurement). Of the 53 500 unique, individual species detected, 13 483 were significantly changed (24%). Figures 3, S2, and S3 and Table S1 show the data generated by these modalities. Integration of data from these platforms facilitated the de novo, time-resolved MOA construction described below.

Phase 3: Mechanism Construction

Comparison of the Empirical Data to a Canonical Cisplatin Mechanism. To evaluate our data set, we generated a canonical MOA consisting of 33 species from a literature survey of transcripts, proteins, and metabolites that change in a variety of cell lines exposed to cisplatin for less than 48 h (Table S2). Figure 4A shows the constructed canonical mechanism;

DOI: 10.1021/acs.jproteome.6b01004
J. Proteome Res. 2017, 16, 1364−1375

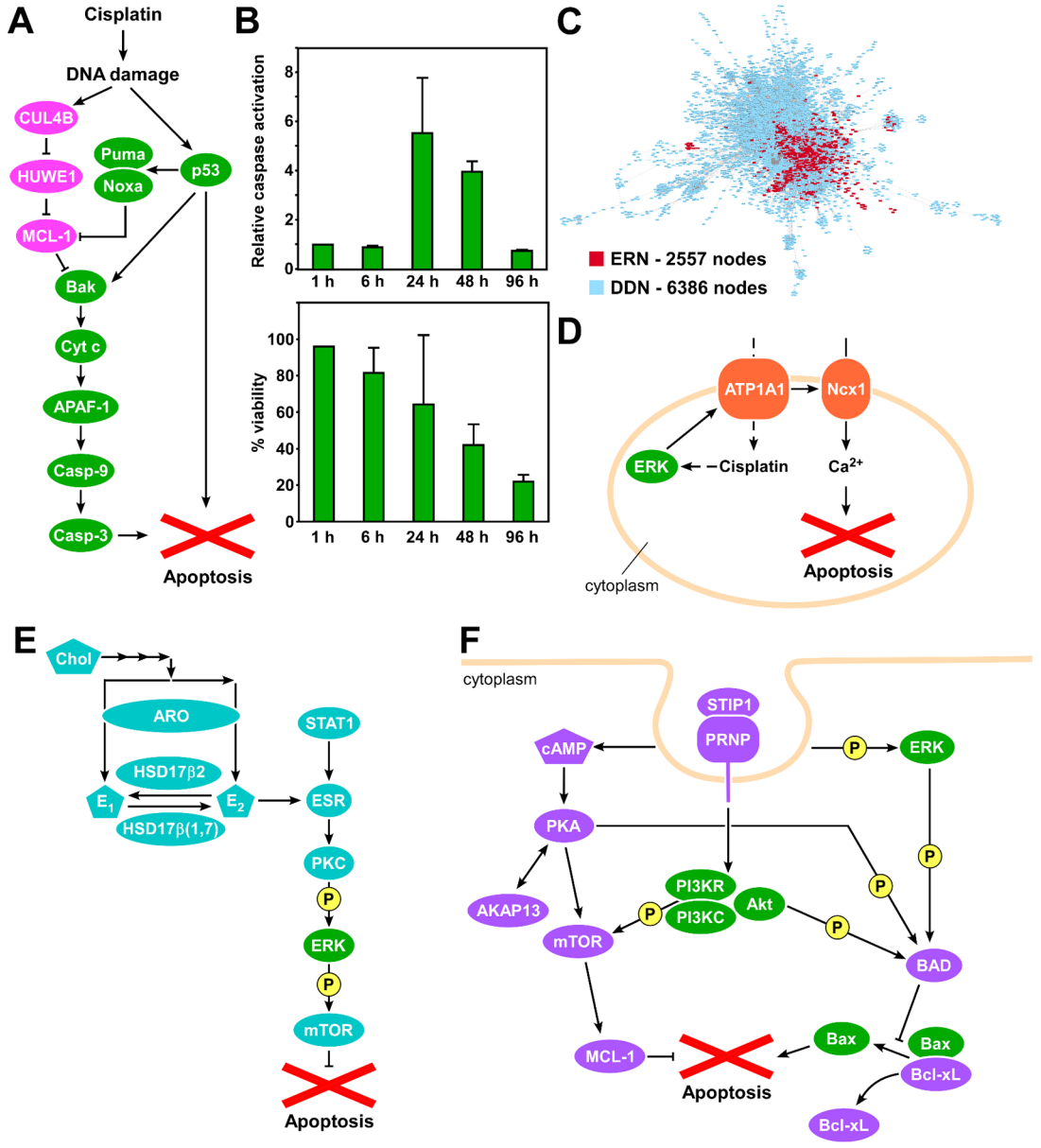

Figure 5. Beyond the primary MOA. (A) The CUL4B/HUWE1 pathway (pink) can modulate the intrinsic apoptosis pathway (green). (B) Relative caspase activation (top) and percent viability (ATP levels; bottom) of 50 μM cisplatin-treated cells compared to untreated cells. (C) Superimposition of the ERN (red) and the DDN (blue) demonstrates capture of known and potentially novel resistance mechanisms. (D) ATP1A1 regulates Ncx1 activity (orange), which can affect the regulation of apoptosis. (E) This pathway illustrates the estrogen-induced cisplatin resistance mechanism (teal). (F) The STIP1 cascade (purple) initiates STIP-1 and PRNP interaction and endocytosis, which ultimately leads to phosphorylation of BAD and inhibition of apoptosis.

cisplatin-induced DNA damage initiates a cellular response that ends in apoptosis. Our multiomics platform detected 97% of the species in the canonical cisplatin MOA (all excepting Mdm2), and 82% of these changed significantly (Table S2).

Figure 4B illustrates time-resolved data for an intrinsic apoptosis pathway within the canonical mechanism. Phosphorylation at Thr202 and Tyr204 activates ERK1; the homologous motif on ERK2 is Thr185/Tyr187. Phosphorylated ERK1 and/or ERK2 increased at each time point. Activated ERK can phosphorylate and activate p53 at multiple sites, including Ser392,[20] which increased significantly in cisplatin-treated cells beginning at 24 h. The literature shows that p53 binds DNA as a tetramer, and phosphorylation at Ser392 enhances tetramer formation 10-fold.[21] Additionally, Chk1 or Chk2 can phosphorylate p53 at Ser313/Ser314. Our data show that p53 pSer313, pSer314, pSer315, or a combination of all three increased significantly in cisplatin-treated cells starting at 6 h. Phosphorylation at these sites can activate *BAX*,[22] consistent with increased detection of the *BAX* transcript in cisplatin-treated cells at 24 h. In intrinsic apoptosis, Bax conformational change in the mitochondrial membrane contributes to cytoplasmic release of Cyt c (*CYCS*) leading to assembly of the apoptosome, which includes APAF-1 and Casp-9, and subsequent Casp-3 activation.[23] We observed transcriptional upregulation in *BAX*, *CYCS*, *APAF1*, and *CASP3* but not proteomic abundance changes for these species, consistent with mediation of their MOA through conformational changes, localizations, and cleavage events. Due to the central role of Casp-9 in the caspase cascade,[24] down-regulation of

DOI: 10.1021/acs.jproteome.6b01004
J. Proteome Res. 2017, 16, 1364−1375

CASP9 at 24 h is consistent with a subpopulation of cells initiating antiapoptotic pathways. By 48 h, none of the downstream apoptosis proteins changed significantly, suggesting that surviving cells were not initiating apoptosis.

Comparison of the Empirical Data to Expanded Mechanisms. Comparison of the measured data to the literature-derived canonical MOA demonstrates agreement both in the network and on a time-resolved basis. However, the capture of 32 out of 33 species from >53 000 unique measurements tests less than 0.1% of the collected data. Thus, further validation of our approach required a strategy that expands beyond the current literature.

We constructed networks by seeding with inputs based on annotated biology, with expansion informed by curated pathways from the Kyoto Encyclopedia of Gene and Genomes (KEGG),[16] allowing us to validate our empirical findings against expected outcomes (see the supplemental methods). The comprehensive nature of multiomics data sets can surpass previously described MOAs. Therefore, we hypothesized that seeding the empirically captured data set would allow us to move beyond these limits and permit exploration of previously unknown but important cellular and pharmacological events associated with the exposure conditions. Figure 4C illustrates this concept. We developed two networks to validate and interrogate our empirical data set: the expanded canonical network (ECN), seeded with species from the canonical mechanism (Table S2), and the data-driven network (DDN), seeded with unique significantly changed species from our empirical data, 11 061 species (Table S3).

The ECN contained 2560 unique species (Figure 4D and Table S4). Our multiomics data set captured 1397 of these (55%), of which 1229 changed significantly. The percentage of unique species that changed significantly in the ECN, 88%, is approximately 3.5 fold higher than the percentage of significantly changed species in the empirical data set (Figure S4). This value is also similar to the percent of significantly changed species determined for the canonical mechanism, validating the primary MOA on the scale of thousands of species and revealing the relevance of the ECN to the cisplatin MOA. Still, the significantly changed multiomics data contains 80% more species than the ECN, providing the opportunity to investigate unexplored pathways related to cisplatin treatment. We hypothesized that these additional measurements revealed previously described and novel off-target effects of cisplatin, including resistance mechanisms.

The resulting DDN had 6386 species (Table S5). We experimentally measured 2583 (40%) of these species, 2215 of which were significantly changed. Similar to the ECN, 86% of the detected species within the DDN changed significantly (Figure S4). For the DDN, limitations to KEGG precluded seeding with metabolomics data and limited the transcriptomic and proteomic data to the 2215 species that were in KEGG (Figure S5). Figure 4D shows the ECN and DDN, with a total of 2560 species (nodes) overlapping. The uncovered DDN region represents intracellular responses not currently understood in the context of cisplatin. As hypothesized, the empirical data set provides the opportunity to explore novel secondary mechanisms.

Beyond the Primary MOA: Capturing the Dynamic Processes that Govern Cell Fate

To complement the DDN analysis and investigate the capability of our platform to capture events outside of the primary MOA, we threaded the empirical data through the Qiagen IPA causal network analysis tool and analyzed for pathways present at every time point. We selected the HUWE1 pathway[25] for further analysis because it appeared as one of the top five ranked hits at every time point and was the top hit at 6 h. The HUWE1 network contained a number of empirically measured species that revealed significant fold changes over time.

HUWE1 is an E3 ubiquitin ligase that modulates DNA damage response and apoptosis pathways upon genotoxic stress.[25] HUWE1 targets MCL-1, an antiapoptotic Bcl2 family member, for ubiquitination and proteasomal degradation; this alleviates MCL-1 repression of Bak and allows Bak to drive pore formation in the mitochondrial outer membrane (Figure 5A). Pore formation induces the release of Cyt c into the cytosol and initiates the caspase cascade. A recent publication shows that up-regulation of CUL4B leads to increased degradation of HUWE1 and subsequent stabilization of MCL-1, which inhibits Bak by forming a heterodimer and ultimately steers the cell away from apoptosis.[26]

We captured regulation of this pathway in a time-resolved manner. The CUL4B C-terminal peptide increased at 1 h with a concomitant significant change in HUWE1 phosphorylation. At 6 h post-exposure CUL4B was unchanged, but we observed evidence for a decrease in HUWE1 phosphorylated and unphosphorylated states. Analysis at 24 and 48 h revealed multiple significant abundance changes for phosphorylated peptides of HUWE1 in treated cells, indicating a dynamic regulation process. Additionally, HUWE1 decreased in abundance at 48 h, suggesting that a population of cells were resistant. Although we did not observe MCL-1 at any time point, *BAK1* increased at 24 h suggesting that a population of cells were committed to apoptosis. The temporal nature of this pathway highlights the dynamic processes at play in the cisplatin-exposed population, with an apparent early up-regulation of pro-survival mechanisms, a later commitment to apoptosis, and detection of an emerging resistant population at 48 h.

Given the dynamic nature of the HUWE1 regulatory circuit, we explored apoptosis and viability pathways using IPA and compared these findings to the empirically derived kinetics of caspase activation and viability. At each time point, IPA sorted significantly changed species in the data set into apoptosis-inhibiting or -activating categories based on their up-regulation or down-regulation and correlation with known functions (Figure S6). The total number of apoptotic proteins increased up to 24 h and declined by 48 h (Figure S6A). However, the ratio of activating to inhibiting molecules remained stable at each time point (52−54%), revealing that not all molecular changes are pro-apoptotic (Figure S6B). We observed similar results when IPA sorted species into viability-inhibiting or -activating categories. The total number of proteins in the viability pathway increased up to 24 h and declined by 48 h, but the ratio of anti- to pro-survival species remained constant (52−57%; Figures S6C and S6D). These trends suggest a heterogeneous population of cells engaged in the dynamic processes of committing to apoptosis or survival.

Consistent with IPA analysis, the measured cellular responses revealed maximal caspase activation at 24 h (Figure 5B). Both IPA analysis and measured cellular data indicate that caspase activation ceased after 48 h. Indeed, the viability data in Figure 5B show a small population of cells (circa 20%) persisted to 96 h, suggesting that these cells represent a cisplatin-resistant population. This prompted us to determine if our platform had captured known and novel resistance mechanisms. Such a capability would provide an early indication of drug resistance

DOI: 10.1021/acs.jproteome.6b01004
J. Proteome Res. 2017, 16, 1364−1375

mechanisms, off-target effects, or both - critical knowledge that could improve clinical trial outcomes.

Construction of Cisplatin Resistance Mechanisms

To validate our capture of resistance mechanisms, we seeded an expanded resistance network (ERN) using the same approach as for the ECN. We identified six proteins in KEGG known to play a role in cisplatin resistance (Table S6). Their expansion resulted in the 1236 species ERN. Our empirical data contained 667 (54%) of these, 589 of which changed significantly (Table S6). Thus, 88% of the empirically detected species in the ERN changed significantly (Figure S4). Figure 5C shows the ERN overlaid on the DDN. The significant overlap of matching nodes validates the presence of known resistance pathways in our data set, consistent with a putatively resistant population at 96 h. Thus, we utilized the ERN to generate testable molecular hypotheses for previously reported resistance proteins.

ATP1A1-Mediated Resistance. ATP1A1, a seed for the ERN and a significantly changed species within our empirical data set, regulates cisplatin uptake into cells and modulates resistance when its expression is suppressed.[27] Interestingly, ATP1A1 also regulates activity of Ncx1.[28] Abrogation of ATP1A1 function concomitantly attenuates Ncx1 activity, which perturbs the calcium signaling pathways of the cell, a phenomenon associated with evasion of apoptosis and implicated in cancer.[29−32] Figure 5D shows the ATP1A1 and Ncx1 pathway. ATP1A1 peptides decreased significantly at 6 and 24 h, consistent with enhanced resistance over time. Ncx1 antisense RNA increased at 1 h, with a significant decrease in the Ncx1 transcript measured at 6 h. At 24 h, both the Ncx1 antisense RNA and the Ncx1 transcript decreased. Reduction of Ncx1 expression and function at these early time points may provide escape avenues by perturbing downstream calcium signaling pathways and disrupting the apoptotic circuit. Recently, disruption of intracellular calcium signaling, tolerance of ER stress, and reduced expression of a subunit of calcium-regulated big potassium channels were implicated in cisplatin resistance.[33,34] Therefore, a better understanding of the pathways that disrupt calcium homeostasis and calcium-regulated apoptotic events is critical to further elucidate cisplatin resistance. Data derived from our multiomics data set for ATP1A1 and Ncx1 present a potential mechanism.

Estrogen-Induced Cisplatin Resistance. Recently, estrogen was shown to mediate resistance to cisplatin-induced apoptosis in A549 cells.[35] Although this study highlighted the importance of caspase attenuation in the mechanism, it did not elucidate a detailed molecular process. The estrogen hormones estrone (E_1) and estradiol (E_2) are synthesized from androgens by aromatase and can also be interconverted by HSD17βs.[36] Additionally, estrogen receptors ESR1 and ESR2 cooperate in promoting early activation of ERK.[37] Examination of the estrogen-related pathways in our data set revealed a transient metabolomic response to cisplatin-induced cytotoxic stress that ultimately leads to a protein-based resistance mechanism. Figure 5E demonstrates a network of events derived de novo from measured molecular changes that potentially lead to resistance through mTOR activation. In cisplatin-treated cells, estrogen species transiently increased: E_1 increased at 1 h, and both E_1 and E_2 increased at 6 h but decreased by 24 h. HSD17β7 increased at 1 h and decreased at 6 h. The transcription factor C/EBPβ, which is activated by cyclic AMP (cAMP)-dependent protein kinase A (PKA),[38] regulates HSD17β dehydrogenase family members.[39] At 24 h, we observed an increase in PKA and in HSD17β7 transcript. E_2 binds to ESR1 and induces PKC-mediated ERK phosphorylation and ERK-dependent mTOR activation.[40,41] We observed ERK phosphorylation at every time point, with mTOR phosphorylation increased at 24 h.

Figure 5E also shows the interaction of STAT1 with ESR leading to mTOR activation. STAT1 overexpression mediates cisplatin resistance in ovarian cancer cell lines through an as yet unexplained mechanism.[42] Activated STAT1 induces the expression of ESR1, feeding into the above-described PKC-ERK mediated activation of mTOR and leading to resistance. Taken together, these data suggest that the STAT1 and estrogen-mediated cisplatin resistance pathways are complementary and that the key elements of the estrogen signaling pathway are activated by 24 h, which may allow escape from cisplatin-induced cytotoxicity by an unique ERK/mTOR axis.

Mining Novel Mechanisms of Cisplatin Resistance

Although the ERN guided identification of associated resistance molecules, pathways outside of the ERN provide the opportunity to discover resistance mechanisms de novo. To explore this, we analyzed the top 20 most dynamically regulated proteins at each time point for potential contribution to mechanisms of resistance and sorted the data based on known links to proliferative capacity or apoptosis.

STIP1 cascade

Figure 5F illustrates a network of events culminating in potential apoptotic escape mechanisms derived de novo from analysis of measured events in the multiomics data set. Based on a dynamic change at 1 h, we identified stress-inducible protein 1 (STIP1) as a putative resistance marker. The DDN associates STIP1 with the prion protein PRNP,[43] which links to the apoptotic activator Bax. Additionally, STIP1 and PRNP associate with cAMP, and activation of the ERK1/2 pathway requires PRNP and STIP1 endocytosis.[44] STIP1 binds to PRNP to drive cell proliferation via activation of the MEK/ERK and PI3K pathways. Collectively, this implicates the PI3K, ERK1/2, and cAMP transduction pathways as downstream modulators of the STIP1-PRNP interaction.

Unification of the synergistic activities of PI3K, ERK1/2, and PKA culminating in BAD phosphorylation presents a novel mechanism elucidated de novo from our empirical data. The right side of Figure 5F illustrates the ERK-mediated signaling events. As previously discussed, increased levels of activated ERK 1/2 were detected at every time point and likely contribute to apoptosis. However, activated ERK can also contribute to antiapoptotic pathways via phosphorylation of BAD, emphasizing its pleiotropic effects. The left side of Figure 5F shows PKA-mediated signaling events. Transcription of catalytic subunits of PKA changed dynamically, with *PRKACA* up-regulated and *PRKACB* down-regulated at 24 h. Functionally, PKA is anchored by binding the AKAP family of proteins, and in our data set, AKAP13 levels as well as phosphorylation states were dynamically regulated at every time point with overall levels up significantly by 48 h. The center of Figure 5F displays PI3K-mediated signaling events.

Within this pathway, we detected a number of significant changes at 24−48 h that were consistent with proliferation in a population of cells. The downstream targets of these pathways, mTOR and BAD, also changed significantly at later time points. Phosphorylated mTOR at pS1166 increased at 24 h. This phosphorylation event was previously identified in response to the pro-proliferative IGF stimulus,[45] consistent with a role in antiapoptotic signaling. Additionally, we detected increased BAD phosphorylation at residues that prevent its binding to

DOI: 10.1021/acs.jproteome.6b01004
J. Proteome Res. 2017, 16, 1364−1375

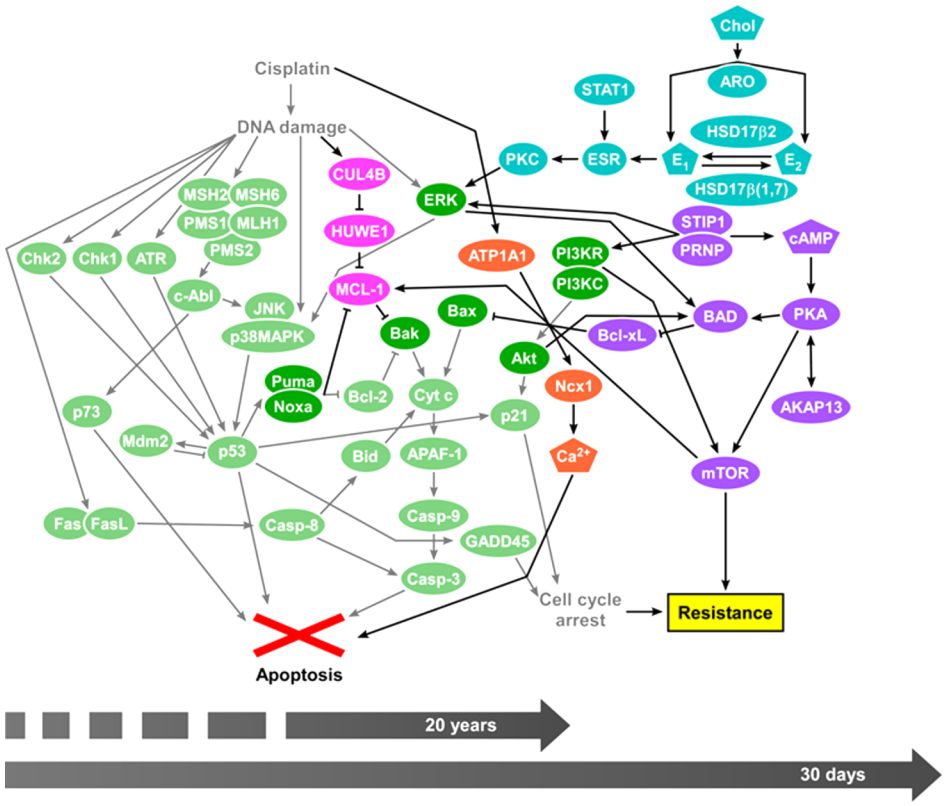

Figure 6. Integrated molecular response to cisplatin perturbation. The cisplatin canonical MOA (green) determined by multiple groups over a 20 year span integrates with the empirically elucidated pathways: CUL4B/HUWE1 pathway (pink); ATP1A1 pathway (orange); STIP1 cascade (purple); and estrogen resistance pathway (teal). Graying represents pathways only from the canonical. The comprehensive mechanism obtained in less than 30 days captures possible resistance.

Bcl-xL/Bcl-2:[46,47] pSer75 (mediated by ERK1/2) at 48 h and pSer118 (mediated by PKA) at 24 h and at 48 h.

Further analysis of the species in these pathways provides insight into cancer development and drug resistance. Overexpression of PRNP in colorectal cancer cells enhances proliferation and attenuates doxorubicin-induced apoptosis.[48] Additionally, PRNP up-regulates the transcriptional activity of β-catenin/TCF4, which inhibits apoptosis upon cisplatin exposure.[49,50] Increased levels of cAMP also confer protection against cisplatin-induced DNA damage and apoptosis, likely through PKA activity.[51] STIP1 is a biomarker for many carcinomas, and it is most commonly associated with ovarian cancers. Cell surface interaction of STIP1 and PRNP was first identified as a neuroprotective event that rescued neurons from apoptosis.[52] Subsequently, it was determined that neuroprotection is mediated by increasing protein synthesis via the PI3K/mTOR signaling axis.[53]

In summary, PI3K, ERK1/2, and cAMP via PKA converge on pro-apoptotic BAD and modulate its phosphorylation. Phosphorylated BAD does not bind and displace Bcl-xL or Bcl-2 from Bak/Bax, preventing Bak/Bax-mediated apoptosis. PI3K and PKA also stimulate mTOR, resulting in stabilization of MCL-1 and further inhibition of the apoptotic pathway by sequestration of Bak.[54,55] As a whole, the STIP1 cascade presented in Figure 5F ultimately targets mTOR and BAD, disrupting both Bak and Bax and protecting the cell from apoptosis through inhibition of pore formation in the mitochondrial outer membrane.

Critical Insight

The pathways identified de novo by our 30 day platform integrate with the canonical cisplatin-induced apoptotic pathway generated from decades of research (Figure 6), suggesting that these findings generate valuable testable hypotheses. These analyses highlight only a few pathways represented in the data set, and further analysis may yield additional hypotheses. This integrated molecular view exemplifies the power of this 30 day multiomics systems biology approach to global MOA analysis for exogenous compounds.

By using network analysis, this platform captures pathways without directly measuring all pathway members. For example, although MCL-1 was not detected, the MCL-1 pathway was identified as important in apoptosis. The MCL-1 pathway is clinically relevant in resistance to Navitoclax, an experimental Bcl2-family inhibitor that does not target MCL-1. Known mechanisms of resistance to Navitoclax directly depend on MCL-1 levels in cells.[56] The current study suggests that systems level analysis of chemotherapeutics has the potential to identify resistance mechanisms and novel pathways controlling apoptosis.

Concluding Remarks and Perspective

The platform described herein utilizes multiomics technologies for large-scale measurement of molecular events to generate a comprehensive picture of the cellular response to an exogenous compound. Using cisplatin, we demonstrate that this platform can identify primary MOA and pathways important for side effects and resistance. This platform provides several key developments in MOA determination. First, a 3 day screening platform determines relevant exposure and dose using MS to determine the maximal molecular changes. Second, comprehensive molecular data are collected within 2−3 weeks, including PTMs and metabolomics. These data can generate a tunable output of the final network or mechanism based on statistical

DOI: 10.1021/acs.jproteome.6b01004
J. Proteome Res. 2017, 16, 1364−1375

confidence in empirical measurements. Finally, this platform provides high-throughput, comprehensive MOA assessment. Previous studies successfully identified compound MOA from published data sets of transcriptional changes in response to compounds.[57,58] Our platform collects post-transcriptional and post-translational data to capture MOA beyond gene regulation.

This technology platform determined the cisplatin MOA beyond previous understanding and annotated interactions, and it provides a framework with which to harness future technological advancements for MOA analysis. However, opportunities exist to enhance these capabilities. Parallel analysis of multiple cell lines will allow MOA determination for various tissue or cell types and provide potential for personalized medicine. Addition of subcellular fractionation and imaging approaches will facilitate detection of mechanistically important translocation events (e.g., Bax, Cyt c). Integration of functional and causal information with the omics data will also provide great value to MOA analysis. Lastly, expansion of database annotation and the tools for data analysis will advance exploration of these multiomic data sets. As technology advances, our strategy will incorporate these enhancements, and further improvements will facilitate data acquisition over hundreds of time points, allowing increased resolution of the empirical MOA and permitting statistical tests of causality.

Apart from these enhancements, our analysis of cisplatin demonstrates that data acquired with this platform provide nearly complete confirmation of the primary MOA for cisplatin cytotoxicity. Furthermore, the data contribute to a more complete description of the biological processes potentially involved in cisplatin resistance. Although these findings require further validation, the results underscore how an integrated omics approach drives the generation of testable hypotheses that directly relate to global cellular responses.

The applications for this platform are diverse and span various fields of study. Assessment of pharmaceutical compounds can rapidly uncover MOA and potential off-target effects as well as improve the selection of drug candidates likely to succeed. This platform could promote rapid MOA assessment for unknown compounds, environmental pollutants, and infectious agents. Additionally, this approach is relevant to the investigation of MOA leading to disease mechanism and developmental abnormalities. Although our present study was performed on monolayer monocultures, it is applicable to suspension cells as well as three-dimensional tissue constructs and organs-on-chips.[59] With this range of applications, this platform is an important resource for characterizing global profiles of the biological processes resulting from cellular perturbations.

■ ASSOCIATED CONTENT

Supporting Information

The Supporting Information is available free of charge on the ACS Publications website at DOI: 10.1021/acs.jproteome.6b01004.

Figures showing cisplatin doses, data increases, estimated sensitivity of SILAC analysis, changes across datasets, KEGG coverage, and IPA analysis. Tables showing experimental data, cisplatin canonical mechanism coverage, data-driven network seed species, expanded canonical network species, data-driven network species, and expanded resistance network species. Additional supplemental experimental procedures. (PDF)

A table containing all measurements and associated information for all modalities. (ZIP)

A table showing canonical and ECN data. (XLSX)

A table showing DDN seed species. (XLSX)

A table showing all species in the ECN. (XLSX)

A table showing all species in the DDN. (XLSX)

Tables showing ERN seed and species data. (XLSX)

■ AUTHOR INFORMATION

Corresponding Author

*E-mail: richard.m.caprioli@vanderbilt.edu.

ORCID

Danielle B. Gutierrez: 0000-0001-6355-2134

Carlos F. Lopez: 0000-0003-3668-7468

John A. McLean: 0000-0001-8918-6419

Jeremy L. Norris: 0000-0003-1725-8406

John P. Wikswo: 0000-0003-2790-1530

Author Contributions

J.L.N., M.A.F., D.B.G., L.D.P., N.M., and S.D.S. are co-first authors. Design was completed by J.L.N., M.A.F., D.B.G., S.D.S., J.M.S., K.L.R., D.B.L., J.A.M., J.P.W., and E.P.S. Sample preparation and instrumentation was completed by J.L.N., M.A.F., D.B.G., S.D.S., J.L.A., J.M.S., A.J., W.B., J.C. Poland, C.R., M.L.M., Y.N., B.M.P., K.L.R., S.H., M.R.K., S.A.R., and N.L. Analysis was completed by J.L.N., M.A.F., D.B.G., L.D.P., N.M., S.D.S., J.C. Pino, J.L.A., J.M.S., A.L.R.L., J.C. Poland, C.F.L., K.L.R., S.H., R.V.P., T.T., N.M.B., M.R.K., J.A.M., and J.P.W. Writing was completed by J.L.N., M.A.F., D.B.G., L.D.P., N.M., S.D.S., J.L.A., J.M.S., A.L.R.L., A.J., W.B., K.L.R., S.H., and R.V.P. Reviewing was completed by J.L.N., M.A.F., D.B.G., L.D.P., N.M., S.D.S., J.C. Pino, J.L.A., J.M.S., A.L.R.L., A.J., W.B., C.R., M.L.M., Y.N., B.M.P., K.L.R., S.H., R.V.P., T.T., C.F.L., D.B.L., J.A.M., J.P.W., E.P.S., and R.M.C. Funding-related work was completed by J.L.N., D.B.L., J.A.M., J.P.W., E.P.S., and R.M.C.

Notes

The authors declare no competing financial interest.

■ ACKNOWLEDGMENTS

Research was sponsored by the U.S. Army Research Office and the Defense Advanced Research Projects Agency and was accomplished under Cooperative Agreement no. W911 NF-14-2-0022. The views and conclusions contained in this document are those of the authors and should not be interpreted as representing the official policies, either expressed or implied, of the Army Research Office, DARPA, or the U.S. Government. The U.S. Government is authorized to reproduce and distribute reprints for Government purposes notwithstanding any copyright notation herein. This work was supported by the National Science Foundation grant MCB-1411482 (C.F.L., J.C.P.) and the VICC Young Ambassador Award (C.F.L.). The authors acknowledge Jerry Holman for assistance in custom coding informatics tools, Randi Gant-Branum for providing valuable feedback to manuscript revisions and the MSRC Proteomics Core at Vanderbilt University for sample services.

■ REFERENCES

(1) Kim, C. Y.; Kim, S. K.; Phi, J. H.; Lee, M. M.; Kim, I. A.; Kim, I. H.; Wang, K. C.; Jung, H. L.; Lee, M. J.; Cho, B. K. A prospective study of Temozolomide plus thalidomide during and after radiation therapy for pediatric diffuse pontine gliomas: preliminary results of the Korean Society for Pediatric Neuro-Oncology study. *J. Neuro-Oncol.* **2010**, *100* (2), 193−198.

DOI: 10.1021/acs.jproteome.6b01004
J. Proteome Res. 2017, 16, 1364−1375

(2) Zhou, Q.; Liao, J. K. Statins and cardiovascular diseases: From cholesterol lowering to pleiotropy. *Curr. Pharm. Des.* **2009**, *15* (5), 467−478.
(3) Hay, M.; Thomas, D. W.; Craighead, J. L.; Economides, C.; Rosenthal, J. Clinical development success rates for investigational drugs. *Nat. Biotechnol.* **2014**, *32* (1), 40−51.
(4) DiMasi, J. A.; Feldman, L.; Seckler, A.; Wilson, A. Trends in risks associated with new drug development: success rates for investigational drugs. *Clin. Pharmacol. Ther.* **2010**, *87* (3), 272−277.
(5) Kola, I.; Landis, J. Can the pharmaceutical industry reduce attrition rates? *Nat. Rev. Drug Discovery* **2004**, *3* (8), 711−715.
(6) Tufts Center for the Study of Drug Development. News. Cost to Develop and Win Marketing Approval for a New Drug Is $2.6 Billion. Available from: http://csdd.tufts.edu/news/complete_story/pr_tufts_csdd_2014_cost_study (accessed February 13, 2016).
(7) Crawford, M. State of the Industry 2010. *News Magazine* **2010**, 34−39.
(8) Scannell, J. W.; Blanckley, A.; Boldon, H.; Warrington, B. Diagnosing the decline in pharmaceutical R&D efficiency. *Nat. Rev. Drug Discovery* **2012**, *11* (3), 191−200.
(9) Pammolli, F.; Magazzini, L.; Riccaboni, M. The productivity crisis in pharmaceutical R&D. *Nat. Rev. Drug Discovery* **2011**, *10* (6), 428−438.
(10) Paul, S. M.; Mytelka, D. S.; Dunwiddie, C. T.; Persinger, C. C.; Munos, B. H.; Lindborg, S. R.; Schacht, A. L. How to improve R&D productivity: the pharmaceutical industry's grand challenge. *Nat. Rev. Drug Discovery* **2010**, *9* (3), 203−214.
(11) Ahuja, V.; Sharma, S. Drug safety testing paradigm, current progress and future challenges: an overview. *J. Appl. Toxicol.* **2014**, *34* (6), 576−594.
(12) Kim, M.-S. Proteomics equipped with multiplexing toward ultra high throughput. *Proteomics* **2015**, *15* (2−3), 183−184.
(13) Sereni, M. I.; Pierobon, M.; Angioli, R.; Petricoin, E. F.; Frederick, M. J. Reverse phase protein microarrays and their utility in drug development. *Methods Mol. Biol.* **2013**, *986*, 187−214.
(14) Lopez, C. F.; Muhlich, J. L.; Bachman, J. A.; Sorger, P. K. Programming biological models in Python using PySB. *Mol. Syst. Biol.* **2013**, *9*, 646.
(15) Cokelaer, T.; Pultz, D.; Harder, L. M.; Serra-Musach, J.; Saez-Rodriguez, J. BioServices: a common Python package to access biological Web Services programmatically. *Bioinformatics* **2013**, *29* (24), 3241−3242.
(16) Kanehisa, M.; Goto, S.; Sato, Y.; Furumichi, M.; Tanabe, M. KEGG for integration and interpretation of large-scale molecular data sets. *Nucleic Acids Res.* **2012**, *40* (D1), D109−D114.
(17) Shannon, P.; Markiel, A.; Ozier, O.; Baliga, N. S.; Wang, J. T.; Ramage, D.; Amin, N.; Schwikowski, B.; Ideker, T. Cytoscape: a software environment for integrated models of biomolecular interaction networks. *Genome Res.* **2003**, *13* (11), 2498−2504.
(18) Yang, Y.; Li, H.; Hou, S.; Hu, B.; Liu, J.; Wang, J. The noncoding RNA expression profile and the effect of lncRNA AK126698 on cisplatin resistance in non-small-cell lung cancer cell. *PLoS One* **2013**, *8* (5), e65309.
(19) Zhang, R.; Li, Y.; Wang, Z.; Chen, L.; Dong, X.; Nie, X. Interference with HMGB1 increases the sensitivity to chemotherapy drugs by inhibiting HMGB1-mediated cell autophagy and inducing cell apoptosis. *Tumor Biol.* **2015**, *36* (11), 8585−8592.
(20) Cheng, Y.; Qiu, F.; Tashiro, S.; Onodera, S.; Ikejima, T. ERK and JNK mediate TNFalpha-induced p53 activation in apoptotic and autophagic L929 cell death. *Biochem. Biophys. Res. Commun.* **2008**, *376* (3), 483−488.
(21) Sakaguchi, K.; Sakamoto, H.; Lewis, M. S.; Anderson, C. W.; Erickson, J. W.; Appella, E.; Xie, D. Phosphorylation of serine 392 stabilizes the tetramer formation of tumor suppressor protein p53. *Biochemistry* **1997**, *36* (33), 10117−10124.
(22) Ou, Y.-H.; Chung, P. H.; Sun, T. P.; Shieh, S. Y. p53 C-terminal phosphorylation by CHK1 and CHK2 participates in the regulation of DNA-damage-induced C-terminal acetylation. *Mol. Biol. Cell* **2005**, *16* (4), 1684−1695.
(23) Taylor, R. C.; Cullen, S. P.; Martin, S. J. Apoptosis: controlled demolition at the cellular level. *Nat. Rev. Mol. Cell Biol.* **2008**, *9* (3), 231−241.
(24) Slee, E. A.; Harte, M. T.; Kluck, R. M.; Wolf, B. B.; Casiano, C. A.; Newmeyer, D. D.; Wang, H. G.; Reed, J. C.; Nicholson, D. W.; Alnemri, E. S.; et al. Ordering the cytochrome c-initiated caspase cascade: hierarchical activation of caspases-2, −3, −6, −7, −8, and −10 in a caspase-9-dependent manner. *J. Cell Biol.* **1999**, *144* (2), 281−292.
(25) Zhong, Q.; Gao, W.; Du, F.; Wang, X. Mule/ARF-BP1, a BH3-only E3 ubiquitin ligase, catalyzes the polyubiquitination of Mcl-1 and regulates apoptosis. *Cell* **2005**, *121* (7), 1085−1095.
(26) Yi, J.; Lu, G.; Li, L.; Wang, X.; Cao, L.; Lin, M.; Zhang, S.; Shao, G. DNA damage-induced activation of CUL4B targets HUWE1 for proteasomal degradation. *Nucleic Acids Res.* **2015**, *43* (9), 4579−4590.
(27) O'Grady, S.; Finn, S. P.; Cuffe, S.; Richard, D. J.; O'Byrne, K. J.; Barr, M. P. The role of DNA repair pathways in cisplatin resistant lung cancer. *Cancer Treat. Rev.* **2014**, *40* (10), 1161−1170.
(28) Swift, F.; Birkeland, J. A. K.; Tovsrud, N.; Enger, U. H.; Aronsen, J. M.; Louch, W. E.; Sjaastad, I.; Sejersted, O. M. Altered Na+/Ca2+-exchanger activity due to downregulation of Na+/K+-ATPase alpha2-isoform in heart failure. *Cardiovasc. Res.* **2008**, *78* (1), 71−78.
(29) Herchuelz, A.; Nguidjoe, E.; Jiang, L.; Pachera, N. Na(+)/Ca (2+) exchange and the plasma membrane Ca(2+)-ATPase in β-cell function and diabetes. *Adv. Exp. Med. Biol.* **2013**, *961*, 385−394.
(30) Hong, S.; Lee, J.; Seo, H.-H.; Lee, C. Y.; Yoo, K.-J.; Kim, S.-M.; Lee, S.; Hwang, K.-C.; Choi, E. Na(+)-Ca(2+) exchanger targeting miR-132 prevents apoptosis of cardiomyocytes under hypoxic condition by suppressing Ca(2+) overload. *Biochem. Biophys. Res. Commun.* **2015**, *460* (4), 931−937.
(31) Markova, J.; Hudecova, S.; Soltysova, A.; Sirova, M.; Csaderova, L.; Lencesova, L.; Ondrias, K.; Krizanova, O. Sodium/calcium exchanger is upregulated by sulfide signaling, forms complex with the β1 and β3 but not β2 adrenergic receptors, and induces apoptosis. *Pfluegers Arch.* **2014**, *466* (7), 1329−1342.
(32) Muñoz, J. J.; Drigo, S. A.; Barros-Filho, M. C.; Marchi, F. A.; Scapulatempo-Neto, C.; Pessoa, G. S.; Guimarães, G. C.; Trindade Filho, J. C. S.; Lopes, A.; Arruda, M. A. Z.; et al. Down-regulation of SLC8A1 as a putative apoptosis evasion mechanism by modulation of calcium levels in penile carcinoma. *J. Urol.* **2015**, *194* (1), 245−251.
(33) Samuel, P.; Pink, R. C.; Caley, D. P.; Currie, J. M. S.; Brooks, S. A.; Carter, D. R. F. Over-expression of miR-31 or loss of KCNMA1 leads to increased cisplatin resistance in ovarian cancer cells. *Tumor Biol.* **2016**, *37* (2), 2565−2573.
(34) Xu, Y.; Wang, C.; Su, J.; Xie, Q.; Ma, L.; Zeng, L.; Yu, Y.; Liu, S.; Li, S.; Li, Z.; et al. Tolerance to endoplasmic reticulum stress mediates cisplatin resistance in human ovarian cancer cells by maintaining endoplasmic reticulum and mitochondrial homeostasis. *Oncol. Rep.* **2015**, *34* (6), 3051−3060.
(35) Grott, M.; Karakaya, S.; Mayer, F.; Baertling, F.; Beyer, C.; Kipp, M.; Kopp, H.-G. Progesterone and estrogen prevent cisplatin-induced apoptosis of lung cancer cells. *Anticancer Res.* **2013**, *33* (3), 791−800.
(36) Thomas, M. P.; Potter, B. V. L The structural biology of oestrogen metabolism. *J. Steroid Biochem. Mol. Biol.* **2013**, *137*, 27−49.
(37) Chimento, A.; Sirianni, R.; Casaburi, I.; Ruggiero, C.; Maggiolini, M.; Andò, S.; Pezzi, V. 17β-Estradiol activates GPER- and ESR1-dependent pathways inducing apoptosis in GC-2 cells, a mouse spermatocyte-derived cell line. *Mol. Cell. Endocrinol.* **2012**, *355* (1), 49−59.
(38) Wilson, H. L.; McFie, P. J.; Roesler, W. J. Characterization of domains in C/EBPalpha that mediate its constitutive and cAMP-inducible activities. *Mol. Cell. Endocrinol.* **2001**, *181* (1−2), 27−34.
(39) Rotinen, M.; Villar, J.; Celay, J.; Serrano, I.; Notario, V.; Encío, I. Transcriptional regulation of type 11 17β-hydroxysteroid dehydrogenase expression in prostate cancer cells. *Mol. Cell. Endocrinol.* **2011**, *339* (1−2), 45−53.
(40) Panchanathan, R.; Shen, H.; Zhang, X.; Ho, S.-M.; Choubey, D. Mutually positive regulatory feedback loop between interferons and estrogen receptor-alpha in mice: implications for sex bias in autoimmunity. *PLoS One* **2010**, *5* (5), e10868.

DOI: 10.1021/acs.jproteome.6b01004
J. Proteome Res. 2017, 16, 1364−1375

(41) Wang, Y.; Zhu, L.; Kuokkanen, S.; Pollard, J. W. Activation of protein synthesis in mouse uterine epithelial cells by estradiol-17β is mediated by a PKC-ERK1/2-mTOR signaling pathway. *Proc. Natl. Acad. Sci. U. S. A.* **2015**, *112* (11), E1382−1391.
(42) Roberts, D.; Schick, J.; Conway, S.; Biade, S.; Laub, P. B.; Stevenson, J. P.; Hamilton, T. C.; O'Dwyer, P. J.; Johnson, S. W. Identification of genes associated with platinum drug sensitivity and resistance in human ovarian cancer cells. *Br. J. Cancer* **2005**, *92* (6), 1149−1158.
(43) Baindur-Hudson, S.; Edkins, A. L.; Blatch, G. L. Hsp70/Hsp90 organising protein (hop): beyond interactions with chaperones and prion proteins. *Subcell. Biochem.* **2015**, *78*, 69−90.
(44) Erlich, R. B.; Kahn, S. A.; Lima, F. R. S.; Muras, A. G.; Martins, R. A. P.; Linden, R.; Chiarini, L. B.; Martins, V. R.; Moura Neto, V. STI1 promotes glioma proliferation through MAPK and PI3K pathways. *Glia* **2007**, *55* (16), 1690−1698.
(45) Patel, B.; Smith, S.; Behling, A.; Conner, K.; Bomgarden, R.; Opperman, K.; Kaboord, B.; Rogers, J. Quantitative analysis of AKT/mTOR pathway using immunoprecipitation and targeted mass spectrometry. https://www.thermofisher.com/content/dam/tfs/ATG/CMD/cmd-documents/sci-res/posters/ms/events/hupo15/PN-64603-LC-MS-AKTm-TOR-Pathway-Immunoprecipitation-HUPO2015-PN64603-EN.PDF (accessed January 6, 2017).
(46) Bansal, N.; Marchion, D. C.; Bicaku, E.; Xiong, Y.; Chen, N.; Stickles, X. B.; Sawah, E. A.; Wenham, R. M.; Apte, S. M.; Gonzalez-Bosquet, J.; et al. BCL2 antagonist of cell death kinases, phosphatases, and ovarian cancer sensitivity to cisplatin. *J. Gynecol. Oncol.* **2012**, *23* (1), 35−42.
(47) Hayakawa, J.; Ohmichi, M.; Kurachi, H.; Kanda, Y.; Hisamoto, K.; Nishio, Y.; Adachi, K.; Tasaka, K.; Kanzaki, T.; Murata, Y. Inhibition of BAD phosphorylation either at serine 112 via extracellular signal-regulated protein kinase cascade or at serine 136 via Akt cascade sensitizes human ovarian cancer cells to cisplatin. *Cancer Res.* **2000**, *60* (21), 5988−5994.
(48) Chieng, C. K.-L.; Say, Y.-H. Cellular prion protein contributes to LS 174T colon cancer cell carcinogenesis by increasing invasiveness and resistance against doxorubicin-induced apoptosis. *Tumor Biol.* **2015**, *36* (10), 8107−8120.
(49) Besnier, L. S.; Cardot, P.; Da Rocha, B.; Simon, A.; Loew, D.; Klein, C.; Riveau, B.; Lacasa, M.; Clair, C.; Rousset, M.; et al. The cellular prion protein PrPc is a partner of the Wnt pathway in intestinal epithelial cells. *Mol. Biol. Cell* **2015**, *26* (18), 3313−3328.
(50) Liu, M.; Yang, S.; Wang, Y.; Zhu, H.; Yan, S.; Zhang, W.; Quan, L.; Bai, J.; Xu, N. EB1 acts as an oncogene via activating beta-catenin/TCF pathway to promote cellular growth and inhibit apoptosis. *Mol. Carcinog.* **2009**, *48* (3), 212−219.
(51) von Knethen, A.; Lotero, A.; Brüne, B. Etoposide and cisplatin induced apoptosis in activated RAW 264.7 macrophages is attenuated by cAMP-induced gene expression. *Oncogene* **1998**, *17* (3), 387−394.
(52) Zanata, S. M.; Lopes, M. H.; Mercadante, A. F.; Hajj, G. N. M.; Chiarini, L. B.; Nomizo, R.; Freitas, A. R. O.; Cabral, A. L. B.; Lee, K. S.; Juliano, M. A.; et al. Stress-inducible protein 1 is a cell surface ligand for cellular prion that triggers neuroprotection. *EMBO J.* **2002**, *21* (13), 3307−3316.
(53) Caetano, F. A.; Lopes, M. H.; Hajj, G. N. M.; Machado, C. F.; Pinto Arantes, C.; Magalhães, A. C.; Vieira, M. D. P. B.; Américo, T. A.; Massensini, A. R.; Priola, S. A.; et al. Endocytosis of prion protein is required for ERK1/2 signaling induced by stress-inducible protein 1. *J. Neurosci.* **2008**, *28* (26), 6691−6702.
(54) de Joussineau, C.; Sahut-Barnola, I.; Tissier, F.; Dumontet, T.; Drelon, C.; Batisse-Lignier, M.; Tauveron, I.; Pointud, J.-C.; Lefrançois-Martinez, A.-M.; Stratakis, C. A.; et al. mTOR pathway is activated by PKA in adrenocortical cells and participates in vivo to apoptosis resistance in primary pigmented nodular adrenocortical disease (PPNAD). *Hum. Mol. Genet.* **2014**, *23* (20), 5418−5428.
(55) Koo, J.; Yue, P.; Deng, X.; Khuri, F. R.; Sun, S.-Y. mTOR complex 2 stabilizes Mcl-1 protein by suppressing its glycogen synthase kinase 3-dependent and SCF-FBXW7-mediated degradation. *Mol. Cell. Biol.* **2015**, *35* (13), 2344−2355.
(56) Konopleva, M.; Contractor, R.; Tsao, T.; Samudio, I.; Ruvolo, P. P.; Kitada, S.; Deng, X.; Zhai, D.; Shi, Y.-X.; Sneed, T.; et al. Mechanisms of apoptosis sensitivity and resistance to the BH3 mimetic ABT-737 in acute myeloid leukemia. *Cancer Cell* **2006**, *10* (5), 375−388.
(57) di Bernardo, D.; Thompson, M. J.; Gardner, T. S.; Chobot, S. E.; Eastwood, E. L.; Wojtovich, A. P.; Elliott, S. J.; Schaus, S. E.; Collins, J. J. Chemogenomic profiling on a genome-wide scale using reverse-engineered gene networks. *Nat. Biotechnol.* **2005**, *23* (3), 377−383.
(58) Woo, J. H.; Shimoni, Y.; Yang, W. S.; Subramaniam, P.; Iyer, A.; Nicoletti, P.; Rodríguez Martínez, M.; López, G.; Mattioli, M.; Realubit, R.; et al. Elucidating compound mechanism of action by network perturbation analysis. *Cell* **2015**, *162* (2), 441−451.
(59) Wikswo, J. P. The relevance and potential roles of micro-physiological systems in biology and medicine. *Exp. Biol. Med.* **2014**, *239* (9), 1061−1072.

DOI: 10.1021/acs.jproteome.6b01004
J. Proteome Res. 2017, 16, 1364−1375